A combined Rayleigh-Raman lidar for measurements of tropospheric water vapour and aerosol profiles (*)

V. RIZI ([1]), M. IARLORI ([1]), P. DI CARLO ([1]), G. VISCONTI ([1]) and G. CINQUE ([2])
([1]) *Dipartimento di Fisica, Università degli Studi - L'Aquila, Italy*
([2]) *Istituto Nazionale di Geofisica, L'Aquila - 67100, Italy*

(ricevuto l'1 Febbraio 1999; revisionato il 27 Settembre 1999; approvato il 21 Ottobre 1999)

Summary. — The receiver of the Differential Absorption Lidar system of the University of L'Aquila (Italy) has been upgraded for the detection of Raman scattering from nitrogen and water vapour induced by XeCl and XeF excimer laser lines. In this configuration, only the XeF source is activated, so we can measure the tropospheric water vapour mixing ratio profiles with a height resolution of 300 m and 10 min in time. The lower limit sensitivity for the mixing ratio of water vapour is about $2 \cdot 10^{-4}$ and the precision ranges between 5% at 2 km and 50% at 9 km. The aerosol back-scattering ratio profiles can be measured with the same altitude and time resolution up to the lower stratosphere, the relative error is below 5% in the troposphere and about 30% at the highest altitudes. Comparisons with coincident PTU balloon-sondes show that the performances of the system in measuring the tropospheric water vapour are well calibrated for studying the water vapour evolution and cloud formation in the troposphere.

PACS 92.60 – Meteorology.
PACS 92.60.Jq – Water in the atmosphere (humidity, clouds, evaporation, precipitation).
PACS 93.85 – Instrumentation and techniques for geophysical research.

1. – Introduction

The water vapour mixing ratio can be a good tracer of the air parcel motion in the atmospheric processes, and a better knowledge of water vapour distribution can lead to an increased understanding of the hydrological cycle in the troposphere, as well as of the radiative processes and of cloud formation. For the latter point the measurements of aerosol content are also important.

In the late 1960s, Cooney *et al.* [1] and Melfi *et al.* [2] have shown that lidars based on the Raman spectroscopy are powerful instruments for the observation of tropospheric water vapour. Although such systems must be calibrated, this technique has been widely used [3-7].

The improvement of lidar systems had fundamental inputs from the technological

(*) The authors of this paper have agreed to not receive the proofs for correction.

advances especially in laser systems; as a consequence, a number of lidars have used the differential absorption technique for water vapour measurements [8, 9], and this approach is very useful for mobile systems, *i.e.*, operating from airborne and space-based platforms, since these systems are self-calibrating.

Other advantages of the Raman scattering approach are that the laser sources do not have to be tuned to a water vapour absorption line and do not require a narrow bandwidth. In addition the Raman lidar water profiling can be coupled with the standard aerosol lidar measurements using the same laser sources [6, 10].

A combined Rayleigh-Raman lidar operates by sending a laser pulse and collecting as a function of time the elastic (Rayleigh and Mie scattering) and inelastic (Raman scattering) back-scattered signals from the atmosphere. The former contains information about the atmospheric density and the aerosol content, the latter allows to discriminate between different species (*i.e.*, water vapour, H_2O, nitrogen, N_2, and oxygen, O_2).

We have improved our differential absorption lidar (DIAL), originally built for the measurement of ozone density profiles [11], with the design and the activation of three additional channels for the detection of the Raman back-scattering from N_2 and H_2O, in addition to the Rayleigh-Mie channels already operating. The operating part of our system allows to measure the tropospheric water vapour and aerosol back-scattering ratio profiles up to 20 km on a time scale of minutes. This feature should give the possibility to study the water vapour time evolution as well as the coupling between water vapour and cloud droplets.

In this work, the details, the performances of the system and the results of a series of observations for the validation of the water vapour measurements are described after a short review of the relevant theory.

2. – Raman scattering in the atmosphere

If an ensemble of photons with a certain wavelength is travelling in a medium constituted of free molecules, there is a significant fraction of the incident photons that are scattered preserving their original wavelength, independently of molecular composition; and a low, but non-zero, fraction of the scattered photons that emerge from the media with shifted wavelengths. The last process is the Raman molecular scattering, the amount of these shifts is the signature of the molecule doing the scattering. Thus different scattering molecules have Raman displacements of different magnitude.

Since in the atmosphere most molecules are in the vibrational ground state, the Stokes bands of Raman spectra (mainly, $\Delta\nu = +1$, where ν labels the vibrational quantum number), with wavelengths longer that the incident light, are much more intense than the corresponding anti-Stokes bands ($\Delta\nu = -1$) at shorter wavelengths. In addition, each vibrational transition gives rise to a closely spaced band of lines corresponding to different rotational transitions, each band contains *S*-, *O*- and *Q*-branches corresponding to different transitions in the rotational quantum number (J); in particular the *Q*-branch ($\Delta J = 0$) constitutes the central part of the band, the *S*-branch ($\Delta J = +2$) is on the side of longer wavelengths and the *O*-branch ($\Delta J = -2$) is on that of shorter wavelength [12].

Focusing on the atmospheric N_2 and H_2O, most of the Raman-scattered photons lie in the part of the spectrum corresponding to the transition ν: $0 \rightarrow 1$. The N_2 vibrational

shift is about 2330.7 cm^{-1} from the exciting frequency and the band of the rotational transition spans around this value. With increasing temperature the rotational band (*S*-, *O*-branches) extends further, but for the atmospheric temperatures (300–200 K), the intensity of the central line (*Q*-branch) remains constant and the width of the rotational bands, which together contribute less than 20% to the total band intensity, ranges below 400 cm^{-1} [13]. The H_2O vibrational shift is about 3652 cm^{-1} [14] and the rotational lines span over a wide range; the *Q*-branch (very narrow, approximately 20 cm^{-1}) is independent of atmospheric temperature and is the only significant contribution to the Raman spectrum.

The density of the Raman back-scattered photons collected with a lidar from different regions of the atmosphere is roughly proportional to the intensity of the laser light, to the number density of the excited molecules, to the atmospheric transmission factors and to the differential Raman back-scattering cross-sections. The latter quantities are about 3 orders of magnitudes lower than the molecular back-scattering cross-sections ($\sim 5.0[\lambda(\mathrm{nm})]^{-4}\cdot 10^{-21}\,m^2\,sr^{-1}$), but they show the same wavelength dependence (λ^{-4}, [15]).

The N_2 differential Raman back-scattering cross-section for the total vibrational-rotational transitions ($\nu: 0 \rightarrow 1$, *S*-, *O*- and *Q*-branches) is about 6.3 $[\lambda_R(\mathrm{nm})]^{-4}\cdot 10^{-24}\,m^2\,sr^{-1}$, where λ_R is the shifted wavelength [16, 17].

For H_2O, the differential Raman back-scattering cross-section is about 2.5 times larger than that of N_2 [18].

3. – System configuration

Since 1991, the ozone Differential Absorption Lidar (DIAL) system of the University of L'Aquila has been operational in routine measurements of aerosols and ozone density profiles [19, 20]. The recent addition of three detector channels does make the system sensitive to the Raman scattering from nitrogen and water vapour. This will provide the opportunity to measure at the same time the aerosol back-scattering profile, the water vapour profile, and the ozone profile [21].

This system is situated at 42.35 °N and 13.38 °E, close to L'Aquila (Italy), and is set up in a monostatic configuration. The transmitter part of the system consists of a XeF excimer laser. The receiving system uses an *f*/10 Cassegrain telescope coupled via a mechanical chopper, field lens and dichroic mirrors to interference filters, photomultipliers and electronic chains for photon-counting. The electronics allows a sampling frequency of 80 MHz, but the photon count rate is kept below 10 MHz, to be sure that the system is linearly responding. The data acquisition is performed with multi-channel scaler cards and a computer. The photon-counting sampling gate is 2 μs large, corresponding to an altitude resolution of 300 m. The characteristics of the system are resumed in table I.

The optical filtering of the received signals has been carefully designed, for separating the various channels (from now on, the various channels are indicated with the central wavelength number, *i.e.*, 382 nm labels the channel detecting the nitrogen Raman lines induced by the XeF laser). The XeF excimer laser emits 3 lines at about 349, 351 and 353 nm, with relative intensity of 0.2, 0.4 and 0.4, respectively [22]; most of the N_2 Raman-scattered photons can be found between about 377 and 387 nm. On the other hand, the main part of H_2O Raman spectra (*Q*-branches) corresponding to the three laser lines spans a region of about 6 nm around 403 nm.

TABLE I. – *Lidar characteristics.*

Sub-system		
Transmitter	Laser	XeF excimer
	Wavelength	351 nm
	Energy per pulse	50 mJ
	Repetiton rate	70 Hz
	Bandwidth	3 lines $\sim$349, $\sim$351, $\sim$353 nm
	Configuration	Unstable resonator
	Divergence (full angle)	$\sim$0.5 mrad
Receiver	Telescope	Cassergrain configuration Zenith pointing
	Diameter	1.0 nm
	f-number	10
	Field of view	0.2–1.0 mrad
	Channels	#3 – 351 nm Rayleigh/Mie scattering (molecules/aerosols) – 382 nm Raman scattering (nitrogen) – 403 nm Raman scattering (water vapour)
Electronics	Data acquisition	Photon counting
	Maximum data rate	10 MHz
	Range resolution	300 m (2 μs)

The lidar overlap function [23] is the same for all the detected channels. The back-scattered radiation collected by the telescope lies on a single optical axis; a series of dichroic mirrors, positioned along this axis, separate, by means of selective reflection

TABLE II. – *Manufactured interference filters.* CWL, BW *and* T *indicate the central wavelength, the bandwidth and the maximum transmission of the filter, the rejection is an estimate of the relative blocking at the position of the other lines.*

Filter/Channel	351 nm Rayleigh/Mie scattering (molecules/ aerosols)	382 nm Raman scattering (nitrogen)	403 nm Raman scattering (water vapour)
CWL (nm)	350.8	382.23	402.82
BW (nm)	10.3	5.02	2.80
T (%)	65	50	50
Rejection	$> 10^4$ at 308 nm $> 10^4$ at 332 nm $> 10^4$ at 382 nm $> 10^4$ at 403 nm	$> 10^7$ at 308 nm $> 10^7$ at 332 nm $> 10^7$ at 351 nm $> 10^7$ at 403 nm	$> 10^7$ at 308 nm $> 10^7$ at 332 nm $> 10^7$ at 351 nm $> 10^7$ at 382 nm

(above 99%), the different part of the spectra containing the Raman and elastically scattered photons.

In front of the photomultipliers, interference filters provide the final filtering of the radiation. The characteristics of the used interference filters are reported in table II. It can be inferred that the measured signal from H_2O Raman back-scattering (channel 403 nm) is relative to the temperature-independent Q-branches arising from the different XeF laser lines, and is collected with an efficiency of about 20%. While the part of the N_2 Raman back-scattered photons (channel 382 nm), suppressed by filtering, contributes less than 1% to the total intensity, and again the collected signal can be assumed temperature-independent. The filtering of the Rayleigh/Mie channels (308 nm and 351 nm) allows the detection of the pure rotational wings.

It should be noted that for all the channels the transmission is acceptable (the transmission of the interference filters is between 30% and 60%). The combination of dichroic mirror reflections and the rejection factors of the interference filters provides a high blocking outside the transmitted bands. The blocking efficiencies are high enough to prevent the corruption of the collected signals, due to the cross mixing among the back-scattered radiation of different wavelengths.

4. – System performances: water vapour mixing ratio and aerosol back-scattering ratio profiles

In the preliminary stage of the system validation and calibration we have activated the XeF laser source: an example of the lidar signals in three operating channels (351, 382 and 403 nm) collected by cumulating about 42000 laser shots (10 minutes) is shown in the top panel of fig. 1.

The overlap between the laser beam and the telescope field of view begins at about 1 km and is complete above 4 km. The H_2O Raman signal is statistically significant up to 10 km; the N_2 Raman and the 351 nm Rayleigh/Mie signals have good signal-to-noise ratios up to 20 km. The enhancement in the 351 nm back-scattering, between 9 and 12 km, indicates the presence of cirrus clouds, their signatures are also evident in the 382 nm Raman channel; this signal shows a greater decrease in the range of clouds due to the increase of the optical density of the atmosphere.

For the setup of our lidar, we can assume that the scattering processes are incoherent, the time constants of the scattering processes are small compared with the laser pulse length and only single scattering contributes to the received signals: the lidar signals can be represented by the usual form [23]:

$$S(z) = \frac{A}{z^2}\,\eta(z)\,\beta(z)\,T(z)\,, \tag{1}$$

where A is a constant, $\eta(z)$ is the altitude-dependent overlap function, $\beta(z)$ is the volume back-scattering coefficient of the active process (Raman or Rayleigh/Mie differential cross-section times the local density of the scatterer), and $T(z)$ is the transmission factor, that depends on the scattering processes integrated over the path of the radiation travelling in the atmosphere (the molecular absorption processes have a marginal role in this spectral range).

The aerosol back-scattering ratio is defined as 1 plus the ratio between the aerosol and molecular volume back-scattering coefficients, and gives an estimation of the

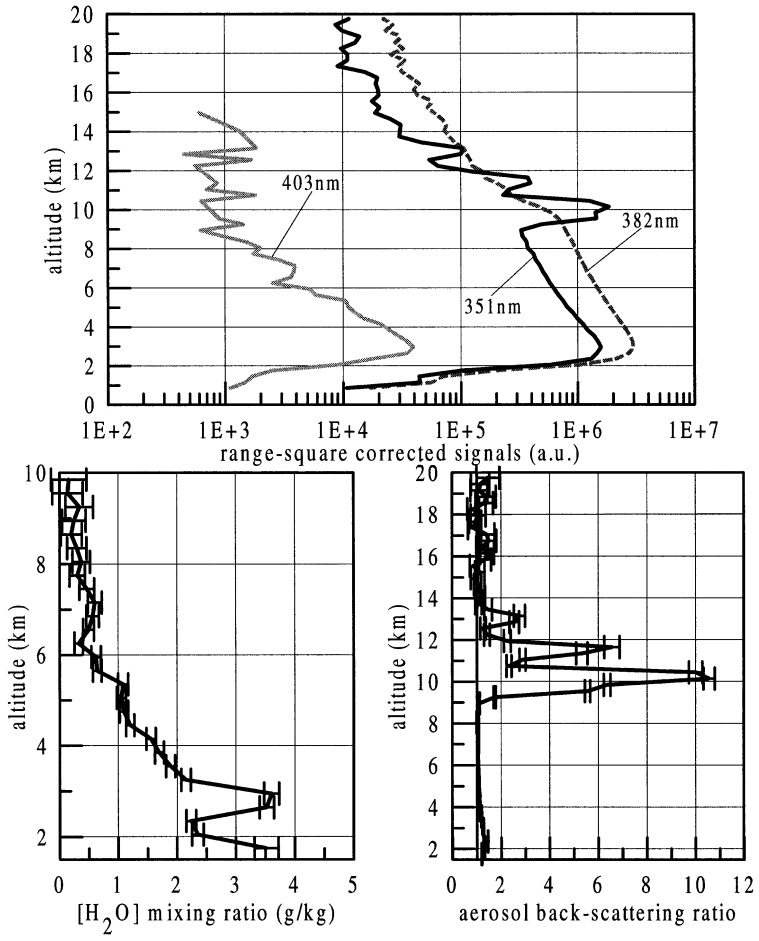

Fig. 1. – Top panel: back-scattering profiles at the three activated channels (19:35UT of 4th March 1998), obtained by accumulating the signals from 42000 laser shots (10 minutes). Bottom panels: the H_2O mixing ratio profile (left) and the aerosol back-scattering ratio (right) retrieved from the lidar signals of the top panel. The uncertainty bars represent an estimate of the one sigma standard errors assuming that the lidar returns are Poisson-distributed.

aerosol mixing ratio; it can be obtained by

$$R(z) = C_{mn} \frac{S_m(z)}{S_n(z)} T_{mn}(z), \tag{2}$$

where S_m is the lidar signal in the 351 nm Rayleigh/Mie channel, C_{mn} is a calibration constant and T_{mn} $(= T_n(z)/T_m(z))$ is the atmospheric differential transmission factor. The calibration constant, C_{mn}, is evaluated by scaling the back-scattering ratio to 1.0 in an altitude region free of aerosols, while $T_{mn}(z)$ can be obtained with an iterative procedure accounting the atmospheric density profile measured by the PTU sonde and the first guess for the aerosol extinction profile and its wavelength dependence [6]. In a

standard measurement (10 minutes) the back-scattering ratio profile between 2 and 20 km is affected by a relative error ranging from 1% below 5 km up to 30% at the highest altitudes.

The water vapour mixing ratio profile is calculated according to

$$w(z) = C_{wn} \frac{S_w(z)}{S_n(z)} T_{wn}(z), \tag{3}$$

where S_w and S_n are the lidar signals in the 403 nm (water) and 382 nm (nitrogen) Raman channels, C_{wn} is a calibration constant accounting for the relative efficiencies of the two channels, $T_{wn}(z)$ $(= T_n(z)/T_w(z))$ is the differential transmission factor including the molecular and aerosol elastic scattering, whose contribution ranges below 10% [6]. $T_{wn}(z)$ is evaluated using the aerosol and the atmospheric density profile. The estimation of C_{wn} is based on the use of coincident local PTU balloon soundings [24], then a water vapour mixing ratio profile is obtained every 10 minutes, from 2 km to 10 km, with a resolution of 300 m, and a precision ranging between 5% and 50%.

The aerosol back-scattering ratio profile retrieved from the lidar signals in the top panel of fig. 1 is shown in the lower right panel. For this case, the lower troposphere is relatively free of aerosols, and a thick cirrus cloud extends between 9 and 14 km, just below the tropopause. The lower left panel of fig. 1 shows the H_2O vapour profiles retrieved from the lidar signals shown in the top panel; the error is below $\pm$ 0.2 grams of water vapour per kilograms of dry air.

Although the telescope field of view and the laser beam are fully overlapped above 4 km, we can retrieve the water vapour and aerosol profiles in the lower range (between 2 km and 4 km), because the altitude-dependent overlap function is the same for all the collected signals.

5. – Preliminary campaign for measurement calibration and validation

With the purpose to validate the overall feasibility of our system in measuring the water vapour profiles, we have arranged comparisons of profiles recorded by the lidar and coincident PTU sondes. Figure 2 displays some of these comparisons carried on during February, March and April 1998.

The altitude-independent calibration constant (C_{wn} in eq. (3)) is estimated by scaling the profile obtained by the lidar to the coincident sonde measurement in a range of altitudes where it is possible to minimise the limitations of the lidar (decreasing precision with increasing range) and of the PTU sonde (unreliable response in relatively dry air, *i.e.*, humidity below 20%).

During this three months campaign, it has been noted that the calibration constant remained the same within $\pm$ 3% [24]. The C_{wn} uncertainty affects the water vapour profile with a relative error below 4%.

We got a quite good correlation between the two techniques, in spite of the fact that the lidar strictly measures over the system site and the balloon sonde drift with the winds and samples different air masses.

The agreement between the measurements taken in clear sky conditions (9th and 11th February and 4th and 17th March 1998) is quite good above 2 km, except for the observation of 4th March 1998: between 2 km and 3 km, the balloon sounding is shifted in altitude with respect to the lidar profile, and this may be due to the

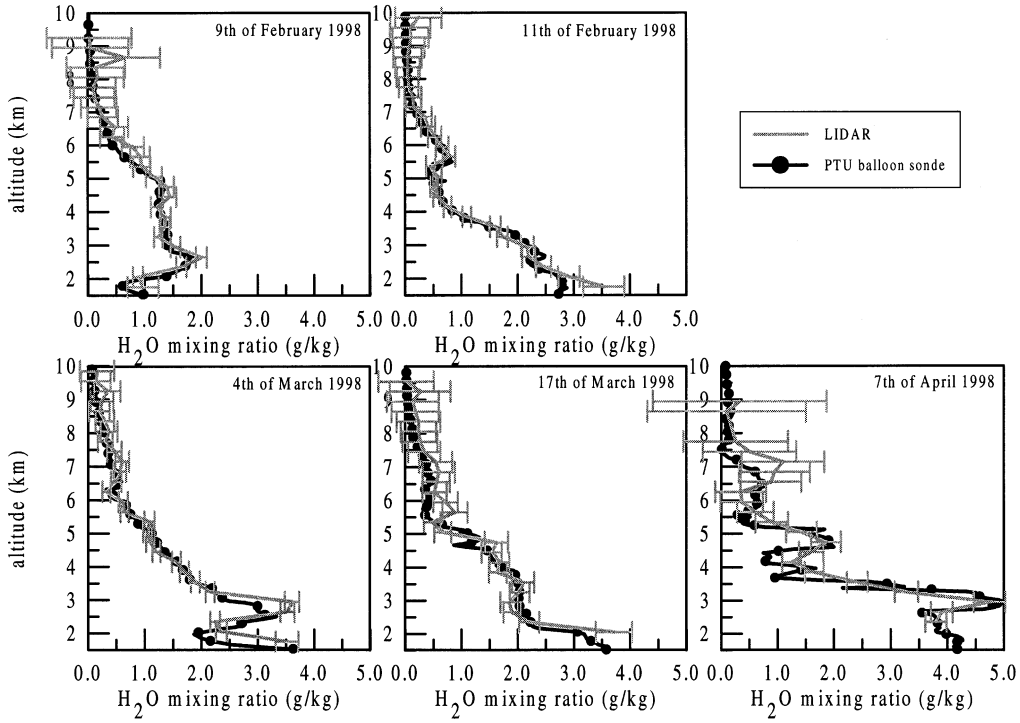

Fig. 2. – Comparisons between water vapour mixing ratio profiles measured with lidar and those of coincident PTU balloon soundings for several observations during February-April 1998.

differences in scaling the balloon sonde geopotential heights to the geometrical altitudes of the lidar profiles.

In addition, it should be considered that the lidar profiling smoothes out the finer structures of the water vapour (possibly present in the PTU *in situ* measurements) due to the limited altitude resolution of our system. On 7th April 1998, there was an optically thin cloud structure between 3 and 4 km; the error is quite large at the higher altitudes due to the decreasing of the atmospheric optical transmission, that degrades the statistical significance of the collected lidar signals.

The bias between lidar and the PTU sonde profiles is on average below $\pm$ 0.2 g/kg, between 3 and 9 km.

6. – Conclusions and perspectives

The new setup of our lidar's receiver allows to measure with standard technique the water vapour mixing ratio profile in the troposphere and the aerosol back-scattering ratio from about 2 km to the lower stratosphere.

Several comparisons of the lidar observations with the *in situ* measurements of water vapour have shown that our system, once calibrated, can provide a water vapour profile with a resolution of 300 m in altitude, averaging the lidar signals accumulated in 10 minutes. The sensitivity of the system is well sized for investigating the temporal

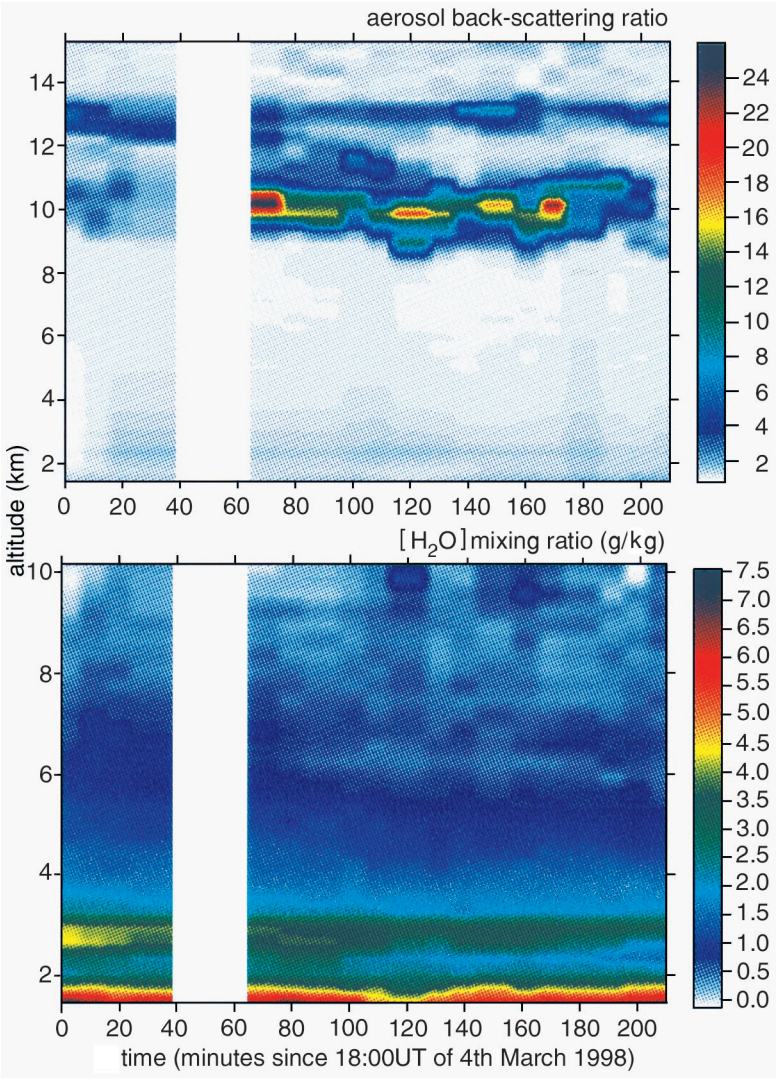

Fig. 3. – Time series of water vapour mixing ratio and aerosol back-scattering ratio profiles. The measurements started at 18:00UT of 4th March 1998. The system was stopped for a fault in the power generators from 18:40UT to 19:05UT. The false colour plates have been obtained by interpolating the adjacent pixels on a grid with the same resolution of the measurements: 300 m in altitude (vertical scales), 10 minutes in time (horizontal scales).

and altitude distribution of water vapour in the local free troposphere and also for estimating the local content of aerosol particles.

An example of the product available after an extended measurement session is shown in the false colour plates in fig. 3. The aerosol back-scattering ratio measurements evidence the local evolution of a multi-layered cirrus cloud, with the lower layer intermittently quite dense. The time and altitude distribution of the water vapour mixing ratio shows features typical of a stratified troposphere. The relatively

high content of water vapour between 2.5 km and 3 km can indicate the persistence of a slowly decreasing thermal inversion. The positions of relative minimum and maximum in the water vapour mixing ratio profile give a rough estimation of the locations of the lower and upper edges of the temperature inversion.

In a coming paper we will investigate the possible correlation between cloud observations in the low troposphere and local water vapour content. The preliminary results allow to speculate about the thermodynamics of cloud formation, and also about the role of Raman scattering by cloud droplets in lidar detection [25].

In this work we focused on the performances of our system in detecting the water vapour and aerosol back-scattering ratio in the troposphere. Actually the activation of elastic channel and of Raman channel corresponding to the XeCl laser source will provide the opportunity to measure also the stratospheric ozone profile.

* * *

This work was partially supported by DG XII of the European Commission under contract No. ENV4-CT95-0090 (SAONAS). The authors thank the Istituto Nazionale di Geofisica for continued assistance. The authors are grateful to V. ARGENTIERI for his contribution to the computing and electronics services, and to O. CONSORTE, F. DEL GRANDE and V. GALLI for their contribution to the design and construction of lidar mechanics. The local balloon soundings are supported by the Consorzio di Ricerca del Gran Sasso. We are also indebted to Prof. V. CUOMO and his staff for their kind cooperation.

REFERENCES

[1] COONEY J. A., *Remote measurements of atmospheric water vapour profiles using the Raman component of laser backscatter, J. Appl. Meteorol.*, **9** (1970) 182-184.

[2] MELFI S. H., LAWRENCE J. D. JR. and MCCORMICK M. P., *Observation of Raman scattering by water vapour in the atmosphere, Appl. Phys. Lett.*, **15** (1969) 295-297.

[3] POURNY J. C., RENAUT D. and ORSZANG A., *Raman-lidar humidity sounding of the atmospheric boundary layer, Appl. Opt.,* **18** (1979) 1141-1148.

[4] MELFI S. H. and WHITEMAN D., *Observation of lower atmospheric moisture structure and its evolution using a Raman lidar, Bull. Am. Meteorol. Soc.*, **66** (1985) 1288-1292.

[5] VAUGHAN G., WAREING D. P., THOMAS L. and MITEV V., *Humidity measurements in the free troposphere using Raman backscatter, Q. J. R. Meteorol. Soc.*, **144** (1988) 1471-1484.

[6] WHITEMAN D. N., MELFI S. H. and FERRARE R. A., *Raman lidar system for the measurement of water vapour and aerosols in the Earth's atmosphere, Appl. Opt.*, **31** (1992) 3068-3082.

[7] GOLDSMITH J. E. M., BISSON S. E., FERRARE R. A., EVANS K. D., WHITEMAN D. N. and MELFI S. H., *Raman lidar profiling of atmospheric water vapour: simultaneous measurements with two collocated systems, Bull. Am. Meteorol. Soc.*, **75** (1994) 975-982.

[8] BROWELL E. V., WILKERSON T. D. and MCILRATH T. J., *Water vapour differential absorption lidar development and evaluation, Appl. Opt.*, **18** (1979) 3474-3483.

[9] GRANT W. B., *Differential absorption and Raman lidar for water vapour profile measurements: a review, Opt. Eng.*, **30** (1991) 40-48.

[10] REICHARDT J., WANDINGER U., SERWAZI M. and WEITKAMP C., *Combined Raman lidar for aerosol, ozone, and moisture measurements, Opt. Eng.*, **35** (1996) 1457-1465.

[11] D'ALTORIO A., MASCI F., VISCONTI G., RIZI V. and BOSCHI E., *Simultaneous stratospheric aerosol and ozone Lidar measurements after the Pinatubo volcanic eruption, Geophys. Res. Lett.*, **19** (1992) 393-396.
[12] HERTZBERG G., *Molecular Spectra and Molecular Structure: I. Spectra of Diatomic Molecules* (Van Nostrand Reinhold) 1968.
[13] INABA H. and KOBAYASI T., *Laser Raman radar-laser Raman scattering methods for remote detection and analysis of atmospheric pollution, Optoelectronics*, **4** (1972) 101-123.
[14] BRIBES J. L., GAUFRES R., MONAN M., LAPP M. and PENNEY C. M., *Raman band contours for water vapour as a function of temperature, Appl. Phys. Lett.*, **28** (1976) 336-337.
[15] SCHRÖTTER H. W. and KLÖCKNER H. W., *Raman scattering cross sections in gases and liquids*, in *Topics in current physics: Raman spectroscopy of gases and liquids*, edited by A. WEBER, Vol. **11** (Springer-Verlag) 1979.
[16] FENNER W. R., HYATT H. A., KELLAM J. M. and PORTO S. P. S., *Raman cross section of some simple gases, J. Opt. Soc. Am.*, **63** (1973) 73-77.
[17] HYATT H. A., CHERLOW J. M., FENNER W. R. and PORTO S. P. S., *Cross section for the Raman effect in molecular nitrogen gas, J. Opt. Soc. Am.*, **63** (1973) 1604-1606.
[18] PENNEY C. M. and LAPP M., *Raman scattering cross sections for water vapour, J. Opt. Soc. Am.*, **66** (1976) 422-425.
[19] D'ALTORIO A., MASCI F., RIZI V., VISCONTI G. and BOSCHI E., *Continuous lidar measurements of stratospheric aerosols and ozone after the Pinatubo eruption. Part I: DIAL ozone retrieval in presence of stratospheric aerosol layers, Geophys. Res. Lett.*, **20** (1993) 2865-2868.
[20] D'ALTORIO A., MASCI F., RIZI V., VISCONTI G. and VERDECCHIA M., *Continuous lidar measurements of stratospheric aerosols and ozone after the Pinatubo eruption. Part II: Time evolution of ozone profiles and of aerosol properties, Geophys. Res. Lett.*, **20** (1993) 2869-2872.
[21] MCGEE T. J., GROSS M. R., SINGH U. N., BUTLER J. J. and KIMVILAKANI P. E., *Improved stratospheric ozone lidar, Opt. Eng.*, **34** (1995) 1421-1430.
[22] BURRIS J. and HEAPS W., *Temporal variations in the spectral output of a xenon fluoride excimer laser, Appl. Opt.*, **34** (1995) 426-427.
[23] MEASURES R. M., *Laser remote sensing: fundamentals and applications* (John Wiley & Sons) 1984.
[24] IARLORI M., *Misure simultanee di vapour d'acqua, ozono ed aerosols*, Tesi di Laurea, Dipartimento di Fisica, Università Degli Studi, L'Aquila, 1998 (available from Università Degli Studi, L'Aquila, Italy).
[25] MELFI S. H., EVENS K. D., LI J., WHITEMAN D. N., FERRARE R. A. and SCHWEMMER G., *Observation of Raman scattering by cloud droplets in the atmosphere, Appl. Opt.*, **36** (1997) 3551-3559.